

Bound and free self-interstitial defects in graphite and bilayer graphene: A computational studyAndris Gulans,^{1,*} Arkady V. Krasheninnikov,^{1,2} Martti J. Puska,¹ and Risto M. Nieminen¹¹*COMP/Applied Physics, Aalto University, P.O. Box 11100, FI-00076 Aalto, Finland*²*Department of Physics, University of Helsinki, P.O. Box 43, FI-00014 Helsinki, Finland*

(Received 6 June 2011; published 15 July 2011)

The role of self-interstitials in the response of layered carbon materials such as graphite, bilayer graphene and multiwalled carbon nanotubes to irradiation has long remained a puzzle. Using density-functional-theory methods with an exchange and correlation functional which takes into account the interlayer van der Waals interaction in these systems without any material-specific empirical parameters, we study the energetics and migration of single- and di-interstitials in graphite and bilayer graphene. We show that two classes of interstitials, “bound” and “free,” can coexist. The latter are mobile at room and lower temperatures, which explains the experimental data and reconciles them with the results of atomistic simulations. Our results shed light on the behavior of graphite and carbon nanotubes under irradiation and have implications for irradiation-mediated processing of bilayer graphene.

DOI: 10.1103/PhysRevB.84.024114

PACS number(s): 81.05.ue, 61.80.-x, 66.30.Lw, 71.15.Mb

I. INTRODUCTION

Structural defects in graphite, a layered material with many applications, has long attracted the attention of the scientific community. Graphite is used in fission reactors, where the Wigner energy stored in irradiation-induced defects is particularly important and calls for atomic understanding of their properties. Although numerous papers on the subject have been published (see Refs. 1 and 2 for an overview), there is still no full microscopic understanding of the behavior of point defects, particularly self-interstitials, in this material.^{3–7} Recent publications on the subject offer very different interpretations of the experimentally observed phenomena.^{8–11} Moreover, the old problem is now also important in the context of the interstitial-type defects in carbon nanotubes (see Refs. 12–15) and bilayer graphene.¹⁶

The lack of a consistent picture can be associated with the difficulties in the interpretation of the experimental data and the accuracy of the results of atomistic simulations. The many types of defects which can exist in graphite make the analysis of the experiments (e.g., annealing of irradiation-induced defects) a formidable task. As for calculations, the main challenge has been the absence of a suitable theoretical model which can accurately describe on equal-footing short-range covalent interactions between carbon atoms within the graphite planes and long-range van der Waals (vdW) interaction between the planes. In all previous density-functional-theory (DFT) simulations either the local-density approximation (LDA) or the generalized-gradient approximation, complemented with an empirical potential (GGA-D), was used. The former approach is not adequate for graphite modeling,¹⁷ and its correct value for the interlayer spacing in graphite is a fortuitous result of error cancellations. Even if this can be tolerated, LDA results are also corrupted by its inaccurate description of covalent bonds.¹⁸ The GGA-D results, in turn, were compromised by the presence of empirical parameters. Moreover, the previous studies focus on stationary states, either leaving behind the details of structural rearrangements or providing a fragmented picture.

In this paper, to avoid the shortcomings described above, we use the nonempirical vdW–density functional (DF) method¹⁹

for an extensive study of the potential energy surface of interstitial-type defects in graphite and bilayer graphene. The vdW-DF method is suitable for systems where weak noncovalent bonds play a crucial role, as it contains an approximation to the nonlocal correlation, which is the origin of the long-range dispersion interactions. We show that at low temperatures, trapped and mobile single interstitials can coexist. The same is true also for the smallest aggregates, di-interstitials. This result explains the mechanism of low-temperature self-diffusion in graphite that has been a mystery for more than a half-century.

II. METHOD AND BENCHMARKS

Calculations were carried out with the VASP code²⁰ using the spin-polarized DFT/projector-augmented wave approach with a plane-wave energy cutoff of 400 eV. Defects are considered in 8×8 and $8 \times 8 \times 2$ supercells of bilayer graphene and graphite, respectively. The Brillouin zone was sampled using only the Γ point. According to our tests with a higher number of \mathbf{k} -points and larger supercells, such a setup allows to obtain defect formation energies with an error of less than 0.04 eV, which is more than adequate knowing the accuracy of DFT methods for chemical reactions²¹ and is sufficient for our purposes.

The nonlocal term in the vdW-DF was evaluated using the adaptive real-space approach.²⁹ The expression of the nonlocal correlation energy in the vdW-DF is well defined. For exchange, we use the semilocal Perdew-Burke-Ernzerhof (PBE)³⁰ description. Such a combination allows one to complement the accuracy of PBE for covalent bonds with appropriate long-range behavior.

Our discussion of the diffusion and structural transformations of carbon interstitials is based on the transition-state (TS) theory. In this framework, the reaction rate k can be expressed using the Arrhenius equation

$$k = A e^{-E_a/k_B T}, \quad (1)$$

where A is the pre-exponential factor and E_a is the activation energy for the process that takes place at temperature T .

While A is of order 10^{13} s^{-1} and typically weakly depends on a reaction, the exponential function is very sensitive to the magnitude of the activation energy. For this reason, we focus on calculating E_a , which we approximate as $E_{\text{TS}} - E_{\text{IS}}$, where E_{TS} and E_{IS} are the potential energies of TS and the initial or (meta)stable state, respectively. A search for TS is performed using the nudged-elastic-band and the dimer algorithms.^{31,32} All TSs and (meta)stable states are obtained using the criterion of magnitudes of forces acting on atoms being less than $0.01 \text{ eV}/\text{\AA}$.

In the present paper, we also investigate the influence of zero-point vibrations (ZPVs) that also contribute to E_a . In that case E_{TS} and E_{IS} are corrected by zero-phonon energies. They are calculated by applying finite displacements of atoms, constructing the dynamical matrix, and finding its eigenfrequencies.

To show that the exchange-correlation functional is appropriately chosen, we test it for bulk graphite and diffusion of adatoms on graphene. Calculated lattice constants, elastic moduli, and exfoliation energies are presented in Table I and compared to results obtained with other methods. As expected, the PBE and vdW-DF with the PBE exchange produce very similar values of lattice constant a and elastic constant $C_{11} + C_{12}$: parameters characterizing intraplanar properties of graphite. The interaction between graphite layers is unphysical within the PBE description and the corresponding properties are not represented in Table I for this method. On the other hand, the calculations show that the vdW-DF(PBE) captures the dispersion interaction and, importantly, reproduces with a great accuracy the experimental values of elastic moduli C_{33} and C_{44} describing the shear and breathing modes between the graphite planes, respectively. Knowing that strain fields of defects including interstitials extend up to hundreds of atoms, even small discrepancies in the elasticity per atom may cause an accumulation of noticeable errors in deformation energies.

Our tests show that the exfoliation energy (the energy per atom necessary for pulling atomic layers of graphite infinitely apart) obtained with the vdW-DF(PBE) is reasonable but not

very accurate. For example, the current benchmark result obtained with the random-phase approximation (RPA) is 1.5 times smaller. However, we are fully convinced that such a discrepancy has a negligible effect on processes studied in the present paper, since a system containing a defect is never compared to another system where an exfoliation takes place.

To summarize, the vdW-DF(PBE) shows a good overall performance for graphite and is excellent particularly for the elastic properties. A much more common version of the vdW-DF, where revPBE³³ is used for the exchange, turns out inferior to our selection for all considered quantities, except for the exfoliation energy, the high accuracy of which is hardly relevant as explained above. Also, the LDA- and GGA-based methods do not offer a noticeable overall improvement over vdW-DF(PBE).

In another test, we use the PBE and vdW-DF(PBE) to calculate the diffusion barrier for a carbon adatom on a single graphene sheet. In the lowest energy configuration the adatom is located above the center of an in-plane bond, and its migration has been studied before in some detail. According to the LDA the corresponding barrier is only 0.1 eV ,^{2,34} while GGA calculations in Ref. 35 predicted 0.47 eV . In our calculation, we obtain 0.45 and 0.44 eV with the PBE and vdW-DF(PBE), respectively. This is consistent with the previous GGA study and also indicates that the vdW-DF(PBE) inherits properties of the PBE as far as chemical bonds are concerned.

III. SINGLE INTERSTITIALS

We considered three fundamental configurations for single self-interstitials (Fig. 1): spiro, grafted and dumbbell interstitials. Their relative stability is determined by the formation energy E_f , which is defined as $E_f = E_{\text{sc}} - N\mu$, where E_{sc} is the total energy of the supercell containing N atoms including the defect. The carbon chemical potential μ is evaluated either for two-layer graphene or for bulk graphite.

TABLE I. Lattice constants a and c , elastic moduli $C_{11} + C_{12}$, C_{33} , and C_{44} and exfoliation energy E_{exf} obtained with various methods.

Method	$a(\text{\AA})$	$c(\text{\AA})$	$C_{11} + C_{12}(\text{GPa})$	$C_{33}(\text{GPa})$	$C_{44}(\text{GPa})$	$E_{\text{exf}}(\text{meV}/\text{atom})$
LDA ^b	2.441	6.660	1283	29.8	–	24.8
LDA ^f	2.45	6.68	1284	29(42)	4.5(4.8)	–
PBE ^d	2.468	–	1245 ^a	–	–	–
GGA-D ^b	2.455	6.690	1265	41.7	–	83.5
GGA-D ^c	2.47	6.6	–	62	–	63
vdW-DF(revPBE) ^d	2.472	7.195	1214 ^a	25	2.0	59
vdW-DF(PBE) ^d	2.470	6.891	1227 ^a	36.4	4.1	71
RPA ^e	2.46	6.68	–	36	–	48
Expt. ^g	2.463	6.712	1248±52	38.7±7.0	5.0±0.3	35±10,52±5

^aExperimental lattice constant c used for a fair comparison of intraplanar elasticity.

^bFrom Ref. 7.

^cFrom Ref. 4.

^dFrom the present paper.

^eFrom Ref. 22.

^fFrom Ref. 23; values in parentheses were obtained using the LCAO-S² + vdW correction.²⁴

^gFrom Refs. 25–28.

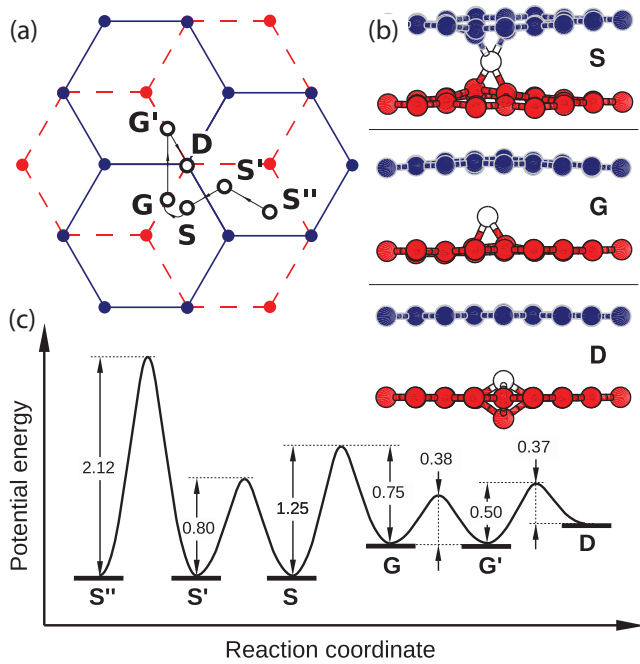


FIG. 1. (Color online) Atomic structures of self-interstitials in graphite. (a) Top view and (b) side view. The labels S, G, and D correspond to the spiro, grafted, and dumbbell configurations, respectively. White circles highlight the interstitials. Blue (dark-gray) and red (gray) circles represent atoms in different layers. (c) The potential energy surface representing the energetics of the configurations and potential barriers (in eV) between them.

Previous papers^{3,6} reported that spirointerstitials are stabilized by macroscopic shear in graphite. We do not elaborate on this topic and consider the single-defect limit by fixing atoms at the borders of our simulation cell in positions that they acquire in the perfect crystal in the AB stacking. Such an alignment of atomic layers leaves the graphite lattice with two inequivalent sites: the α site, where an atom is located right above an atom of the adjacent layer; and the β site, where an atom is located above the center of a hexagon of the adjacent layer.

The formation energies of the interstitial defects at low concentrations are listed in Table II. The energetic hierarchy remains the same regardless of whether graphite or bilayer graphene is considered. Consistently with previous studies,^{3,4,6} the most stable structure is the spirointerstitial, while the dumbbell interstitial is the least stable. The picture does not change if the formation energy is corrected for ZPVs. According to our phonon calculations, the magnitude of the correction is within the range -0.14 to -0.25 eV, which shows that ZPVs cannot be ignored when energy differences of ~ 0.1 eV are important.

The formation energies obtained for bilayer graphene are lower than those for bulk graphite by roughly 0.2 eV, with the difference being only slightly dependent on the type of the interstitial. This observation is explained by steric effects, namely, extra layers in graphite restrict the out-of-plane deformations of the layers adjacent to the defect. As a result, the interstitials in bulk find themselves under pressure in less favorable positions, with strained and hence weaker

TABLE II. Formation energies (eV) of single interstitials. Values corrected for zero-point vibrations are given in parentheses.

Structure	Method	S	G	D
Bilayer	vdW-DF	6.59	7.09	7.21
		(6.45)	(6.84)	(6.96)
Bulk	vdW-DF	6.76	7.27	7.41

chemical bonds, than in a bilayer. This logic is also applicable to interstitials in a supported graphene bilayer, where the substrate plays the same role as the additional layers in bulk graphite. With a qualitative understanding of the steric effects, we restrict our discussion of migration and structural transformations to defects in bilayer graphene only. The considered processes and the corresponding potential energy barriers are shown in Fig. 1.

We found that the diffusion of spirointerstitials can be described by three processes. (i) In transition $S' \rightarrow S$, one of the four bonds linking the interstitial to adjacent graphene layers breaks. This corresponds to the short-range type of migration when the spirointerstitial is pinned to an α site. (ii) The transition $S'' \rightarrow S'$ is a process where a spirointerstitial moves from one α site to another and, hence, corresponds to the long-range migration. It requires that two bonds be broken during the event, hence the corresponding barrier of 2.12 eV is too high for this process to be a matter of interest. (iii) The transformation $S \rightarrow G$ brings the spirointerstitial to the grafted structure, which has the relatively low migration energy of 0.38 eV (lower by 0.06 eV than for an adatom on graphene), which decreases to 0.31 eV if ZPVs are taken into account. The grafted interstitial is very mobile and its migration is not restricted to any area. The grafted structure also easily transforms to the dumbbell configuration, which is the key process for diffusion along the c axis.⁴

The described migration patterns leave no room for the low-temperature diffusion of spirointerstitials. The process with the lowest activation where such a defect is involved is a circular motion around the α site. Due to the relatively high activation energy of 0.80 eV, it becomes important only above room temperature. The long-range transport of spirointerstitials requires even higher temperatures, as shown in scenario iii.

In historical terms, spirointerstitials with a low mobility can be associated with the bound interstitial model, while grafted interstitials, with their low migration energy, behave as if they were free. Note that in the older literature, interstitials were commonly considered to be free, namely, they did not have any covalent bonds with the graphene sheets, which is not consistent with results of modern electronic structure calculations including ours.

If a graphite sample is irradiated at temperatures below 80 K as in Refs. 36 and 37, it is very likely that many interstitials will be in other than the lowest-energy configuration. For instance, if an interstitial is trapped in the grafted configuration, it has to overcome a barrier of 0.75 eV to reach the most stable state. The rate of the process is extremely low at such temperatures. More specifically, according to Eq. (1), the transition $G \rightarrow S$ takes significantly more time than the age

of the Earth and is 10^{23} times less frequent than the transition $S \rightarrow S'$ at 80 K. Under such conditions the transformation of the grafted interstitial to the lowest-energy configuration is a negligible process and we anticipate the coexistence of different interstitial types. Thus our results provide the evidence that graphite irradiated at low temperatures should contain both “bound” (spiro) and “free” (grafted) interstitials.

IV. DI-INTERSTITIALS

As a consequence of interstitial migration or even directly under irradiation, the defects can form bound pairs: di-interstitials. The variety of structures is rich,^{7,11} but we consider only those di-interstitials shown in Fig. 2, as they are the most interesting for the present discussion.

The formation energies of the di-interstitials are listed in Table III. The difference between the values obtained for bilayer and bulk structures is 0.41–0.74 eV. It is significantly larger than that obtained for single interstitials, which means that a carbon dimer takes more space between graphene layers and causes more lattice distortions than a single atom. The spread of the differences in the di-interstitial case indicates that the energetics of transformations is influenced by the number of layers in the system. Due to the high amount of the computational effort, our discussion is restricted to various processes that take place in the bilayer graphene. However, we expect that they reflect general trends that are also valid in the bulk.

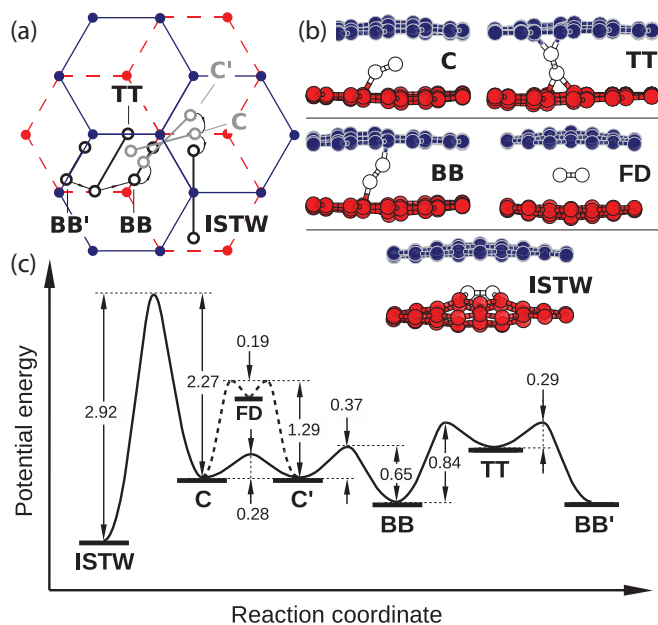


FIG. 2. (Color online) Atomic configurations of di-interstitials and energetics of their transformations. (a) Top view and (b) side view. The labels C, TT, BB, FD, and ISTW correspond to the crane, twin-triangle, bent-bridge, free-dimer, and inverse Stone-Thrower-Wales di-interstitials, respectively. White circles highlight the interstitial atoms. Blue (dark-gray) and red (gray) circles represent atoms in different layers. (c) The potential energy surface representing the energetics of the configurations and potential barriers (in eV) between them.

TABLE III. Formation energies (eV) of di-interstitials

Host	C	TT	BB	FD	ISTW
Bilayer	8.51	8.73	8.17	9.56	7.86
Bulk	9.21	9.14	8.93	10.50	8.60

As in Refs. 7 and 11, we found that the lowest-energy di-interstitial is the inverse Stone-Thrower-Wales (ISTW).³⁸ According to our TS calculations, it is separated from other structures by the high energy barrier of 2.27 eV, which means that two or more types of di-interstitials can coexist over a certain range of temperatures.

Unlike the ISTW, other considered structures are mobile at room or even liquid nitrogen temperature due to the relatively low energy cost of rebonding. Similarly to single interstitials, one can outline several diffusion scenarios.

(1) At very low temperatures the most likely candidate for diffusion is the free-dimer structure. Since its motion does not require breaking of any chemical bonds, the energy barrier of this process is very small, only around 0.03 eV.

(2) The crane structure contains one carbon atom that is not directly bound to adjacent layers. The transition $C \rightarrow C'$ involves the breaking of one bond, and in TSs the carbon dimer is completely detached. Hence the corresponding migration energy is higher than for the previous process, at 0.28 eV. Note that this value is lower than the activation energy for a transformation to any other structure. Provided the temperature is high enough, this process is frequent and can take place many times before the crane di-interstitial becomes trapped in the bent-bridge state.

(3) If a di-interstitial is stuck in the bent-bridge configuration, it requires 0.65 eV to transform into the crane structure. Then the process continues as described in scenario 2, above, until the defect becomes trapped again. In this sequence, $BB \rightarrow C \rightarrow C' \rightarrow \dots \rightarrow C^{(n)} \rightarrow BB'$, the bottleneck is the first reaction. Once it takes place, the di-interstitial is likely to travel for a long while before the process $BB \rightarrow C$ must occur again. Assuming that the pre-exponential factors for $C \rightarrow C'$ and $C \rightarrow BB$ are the same, the ratio for the reaction rates is $\exp[(E_{C \rightarrow BB} - E_{C \rightarrow C'})/k_B T]$. For instance, at $T = 80$ K and $T = 300$ K, there are 4.6×10^5 and 32 $C \rightarrow C'$ events per 1 $C \rightarrow BB$ event, respectively. Remarkably, this seemingly small energy difference, 0.09 eV, leads to an enormous difference in the reaction rates.

(4) A different route for a migration from the bent-bridge state is the path $BB \rightarrow TT \rightarrow BB'$. Compared to the above process, it is much slower, as the activation energy of its bottleneck reaction is higher and has to occur in every migration event.

The processes described involve two structures that have not been obtained in DFT calculations in previous works. One of them, the free-dimer di-interstitial, has been a matter of debate in very recent works.^{8–10} Here, we show that such a metastable structure does exist. It easily binds to any of the adjacent graphene layers, and the activation energy of this process is 0.19 eV. It is clear that the free dimer cannot survive temperatures above that of liquid nitrogen. The other structure previously ignored is the crane di-interstitial,

although its formation energy is relatively low and the structure resembles adatom dimers obtained for graphene in Ref. 7.

The results obtained are important for the correct interpretation of a number of experiments conducted during the last half-century. The explanation of the annealing peaks at temperatures below 180 K and, most notably, at 80 K were initially related to the processes triggered by diffusion of unbound interstitials with a migration energy of up to 0.2 eV.¹ After DFT calculations of reasonably sized systems became feasible, the discovery of the ground-state structure and related energetics caused denial of this model. Telling and Heggie provided alternative explanations relating the low-temperature energy releases to local structural rearrangements of defects or basal dislocation motion.⁵ On the contrary, our calculations show that even single interstitials can be involved in low-energy processes. The obtained migration energy, 0.31 eV, is comparable to the values 0.1–0.4 eV suggested in experimental studies.¹

Despite the proven mobility of certain species of di-interstitials, the significance of each di-interstitial state in this picture is not clear, due to the lack of knowledge of which specific structures are formed immediately after the impact of energetic particles, and in what proportions. On the other hand, our test calculations show that the formation of the mobile crane structure is likely upon merging of two single interstitials, which boosts the aggregation of the defects into larger interstitial clusters.

V. CONCLUSIONS

In conclusion, we have carried out DFT simulations of single and di-interstitials in graphite and bi-layer graphene with an exchange and correlation functional which takes into account the vdW interaction without any material-specific parameters. We have calculated the energetics of different defect configurations and energy barriers between them. We have shown that there are two types of single and di-interstitials, with different migration energies, which can be referred to as “bound” and “free.” The latter can exist after low-temperature irradiation of graphite, so that the results of numerous experiments^{1,36,37} on graphite irradiation can be explained and reconciled with the contradicting results of atomistic simulations.² Our results also shed light on the behavior of interstitials in bi-layer graphene and, keeping in mind the effects of the finite curvature, in multiwalled carbon nanotubes as well, and should be taken into account when irradiation is used to tailor the properties of these structures.

ACKNOWLEDGMENTS

We thank C. Latham for useful discussions. This work was supported by the Academy of Finland through the Centre of Excellence and other projects. We also acknowledge the Finnish IT Center for Science for generous grants of computer time.

*Corresponding author: agl@cc.hut.fi

- ¹P. A. Thrower and R. M. Mayer, *Phys. Status Solidi A* **47**, 11 (1978).
- ²R. H. Telling and M. I. Heggie, *Philos. Mag.* **87**, 4797 (2007).
- ³L. Li, S. Reich, and J. Robertson, *Phys. Rev. B* **72**, 184109 (2005).
- ⁴Y. Ma, *Phys. Rev. B* **76**, 075419 (2007).
- ⁵R. H. Telling, C. P. Ewels, A. A. El-Barbary, and M. I. Heggie, *Nat. Mater.* **2**, 333 (2003).
- ⁶T. Teobaldi, H. Ohnishi, K. Tanimura, and A. L. Shluger, *Carbon* **48**, 4145 (2010).
- ⁷G. Teobaldi, K. Tanimura, and A. L. Shluger, *Phys. Rev. B* **82**, 174104 (2010).
- ⁸T. Iwata and M. Watanabe, *Phys. Rev. B* **81**, 014105 (2010).
- ⁹C. D. Latham, G. L. Haffenden, M. I. Heggie, I. Suarez-Martinez, and C. P. Ewels, *Phys. Rev. B* **82**, 056101 (2010).
- ¹⁰T. Iwata and M. Watanabe, *Phys. Rev. B* **82**, 056102 (2010).
- ¹¹C. D. Latham, M. I. Heggie, J. A. Gamez, I. Suarez-Martinez, C. P. Ewels, and P. R. Briddon, *J. Phys. Condens. Matter* **20**, 395220 (2008).
- ¹²A. V. Krasheninnikov and F. Banhart, *Nat. Mater.* **6**, 723 (2007).
- ¹³A. V. Krasheninnikov and K. Nordlund, *J. Appl. Phys.* **107**, 071301 (2010).
- ¹⁴B. Peng, M. Locascio, P. Zapol, S. Li, S. L. Mielke, G. C. Schatz, and H. D. Espinosa, *Nat. Nano* **3**, 626 (2008).
- ¹⁵S. Mathew, U. Bhatta, J. Ghatak, B. Sekhar, and B. Dev, *Carbon* **45**, 2659 (2007).

- ¹⁶E. Cruz-Silva, A. R. Botello-Méndez, Z. M. Barnett, X. Jia, M. S. Dresselhaus, H. Terrones, M. Terrones, B. G. Sumpter, and V. Meunier, *Phys. Rev. Lett.* **105**, 045501 (2010).
- ¹⁷F. Tournus, J. Charlier, and P. Mélinon, *J. Chem. Phys.* **122**, 094315 (2005).
- ¹⁸L. A. Curtiss, K. Raghavachari, P. C. Redfern, and J. A. Pople, *J. Chem. Phys.* **106**, 1063 (1997).
- ¹⁹M. Dion, H. Rydberg, E. Schröder, D. C. Langreth, and B. I. Lundqvist, *Phys. Rev. Lett.* **92**, 246401 (2004).
- ²⁰G. Kresse and J. Furthmüller, *Phys. Rev. B* **54**, 11169 (1996).
- ²¹J. Zheng, Y. Zhao, and D. G. Truhlar, *J. Chem. Theory Comp.* **3**, 569 (2007).
- ²²S. Lebègue, J. Harl, T. Gould, J. G. Ángyán, G. Kresse, and J. F. Dobson, *Phys. Rev. Lett.* **105**, 196401 (2010).
- ²³G. Savini, Y. Dappe, S. Berg, J.-C. Charlier, M. Katsnelson, and A. Fasolino, *Carbon* **49**, 62 (2011).
- ²⁴Y. J. Dappe, M. A. Basanta, F. Flores, and J. Ortega, *Phys. Rev. B* **74**, 205434 (2006).
- ²⁵A. Bosak, M. Krisch, M. Mohr, J. Maultzsch, and C. Thomsen, *Phys. Rev. B* **75**, 153408 (2007).
- ²⁶L. A. Girifalco and R. A. Lad, *J. Chem. Phys.* **25**, 693 (1956).
- ²⁷L. X. Benedict, N. G. Chopra, M. L. Cohen, A. Zettl, S. G. Louie, and V. H. Crespi, *Chem. Phys. Lett.* **286**, 490 (1998).
- ²⁸R. Zacharia, H. Ulbricht, and T. Hertel, *Phys. Rev. B* **69**, 155406 (2004).
- ²⁹A. Gulans, M. J. Puska, and R. M. Nieminen, *Phys. Rev. B* **79**, 201105 (2009).

- ³⁰J. P. Perdew, K. Burke, and M. Ernzerhof, *Phys. Rev. Lett.* **77**, 3865 (1996).
- ³¹H. Jónsson, G. Mills, and K. W. Jacobsen, *Nudged Elastic Band Method for Finding Minimum Energy Paths of Transitions in Classical and Quantum Dynamics in Condensed Phase Simulations* (World Scientific, Singapore, 1998), p. 385.
- ³²J. Kästner and P. Sherwood, *J. Chem. Phys.* **128**, 014106 (2008).
- ³³Y. Zhang and W. Yang, *Phys. Rev. Lett.* **80**, 890 (1998).
- ³⁴M. Heggie, B. R. Eggen, C. P. Ewels, P. Leary, S. Ali, G. Jungnickel, R. Jones, and P. R. Briddon, *Recent Advances in the Chemistry and Physics of Fullerenes and Related Materials*, vol. 6, edited by K. M. Kadish and R. S. Ruoff (Electrochemical Society: Pennington, NJ, 1998), pp. 60–67.
- ³⁵P. O. Lehtinen, A. S. Foster, A. Ayuela, A. Krasheninnikov, K. Nordlund, and R. M. Nieminen, *Phys. Rev. Lett.* **91**, 017202 (2003).
- ³⁶S. B. Austerman and J. E. Hove, *Phys. Rev.* **100**, 1214 (1955).
- ³⁷M. Lucas and E. Mitchell, *Carbon* **1**, 345 (1964).
- ³⁸M. T. Lusk and L. D. Carr, *Phys. Rev. Lett.* **100**, 175503 (2008).